JTTEE5 15:827-833
DOI: 10.1361/105996306X146992
1059-9630/$19.00 © ASM International

Nozzle Developments for Thermal Spray at Very Low Pressure

Rodolphe Bolot, Dmitri Sokolov, Didier Klein, and Christian Coddet

(Submitted February 20, 2006; in revised form April 19, 2006)

Very low pressure plasma spraying has been the object of numerous studies for the past years. However, numerical simulations and experiments revealed some difficulties such as the presence of successive expansions and constrictions of the plasma jet that have an influence on the deposition efficiency and on the coating structure. Optimization of the plasma gun is thus required and the use of bell-contoured De Laval nozzle extensions seems particularly promising. In this paper, new developments concerning the use of an in-house bell-contoured nozzle extension are presented, and both numerical calculations and experiments were performed.

Keywords bell-contoured nozzle, clogging, low pressure, plasma spray, powder injection, thermal losses

1. Introduction

Very low pressure plasma spraying is a way to bridge the gap between physical vapor deposition (PVD) and low-pressure plasma spray (LPPS) processes while preserving the high deposition rate of the latter. Conventional LPPS equipments are usually designed for a chamber pressure of a few tens of mbar. Since the objective of very low pressure plasma spray is to deposit coatings at pressure levels as low as 1 mbar, conventional equipment is not suitable anymore. For example, the use of the standard F4VB gun (Sulzer-Metco, Switzerland) produces an underexpanded plasma jet so that successive expansions and constrictions take place in the vacuum chamber. Hence, modifications of the diverging angle and of the nozzle exit diameter have to be considered. However, these changes do not allow producing a unidirectional plasma jet either. For this, the use of a bell-contoured De Laval type diverging nozzle is required. The idea of using a nozzle extension was recently proposed (Ref 1). More precisely, a lengthened F4 type nozzle provided by MEDICOAT AG (Switzerland) was used with a fastened in-house designed nozzle extension. The nozzle extension was a bell-contoured De Laval type using a larger exit diameter and a longer length compared with those of the standard F4VB gun. The bell-contoured nozzle used in this study presents a throat diameter of 5 mm, an exit diameter of 27 mm, and a divergent length of 80 mm. The method used for the design of the nozzle contour is based on an extension of the theory of Foelsch (Ref 2) that was described in Ref 1. An improvement in the jet uniformity was expected and obtained. However, the choice of the injection point was identified as an additional key parameter. In particular, for the first set of experiments performed with an injection point placed close to the nozzle throat, a partial clogging of the nozzle extension was observed for whatever the carrier flow rate used. On the contrary, if the injection point is placed close to the exit of the nozzle extension, the thermal power available in the plasma jet becomes too low and is too much dispersed to allow a good melting of the injected particles. In fact, due to the cooling of the lengthened constant diameter part of the nozzle and of the diverging extension, the part of the electrical energy extracted by the cooling water circuits becomes very important. For these reasons, the authors' last experiments (Ref 3) were performed using a conventional nozzle despite the previously mentioned drawbacks.

In this paper, the length of the constant diameter extension was reduced to a minimum (2 mm) to decrease thermal losses. Moreover, particular attention was paid to the powder injection point and the injection modeling was performed by considering different axial positions. Figure 1 shows the lengthened nozzle (the blue part of Fig. 1) equipped with the bell-contoured extension (the yellow part of Fig. 1) as it was first used (Ref 1). The initial length of the constant diameter nozzle extension was 30 mm.

Fig. 1 View of the lengthened F4 type nozzle provided by MEDICOAT AG and equipped with an in-house designed bell-contoured extension (the yellow part)

This article was originally published in *Building on 100 Years of Success, Proceedings of the 2006 International Thermal Spray Conference* (Seattle, WA), May 15-18, 2006, B.R. Marple, M.M. Hyland, Y.-Ch. Lau, R.S. Lima, and J. Voyer, Ed., ASM International, Materials Park, OH, 2006.

Rodolphe Bolot, Dmitri Sokolov, Didier Klein, and **Christian Coddet,** LERMPS, Université de Technologie de Belfort-Montbéliard, Site de Sévenans, 90010 Belfort Cedex (France). Contact e-mail: rodolphe.bolot@utbm.fr.

Fig. 2 View of the shortened F4 type nozzle (the blue part) equipped with the in-house bell-contoured diverging extension

Fig. 3 CAD view of the additional water circuit brazed around the De Laval nozzle extension

2. Design Enhancements

2.1 Nozzle Shortening

Figure 2 presents the MEDICOAT extended nozzle (the blue part of Fig. 1) that was shortened by 28 mm to decrease thermal losses in the cooling water circuit. In fact, this modification may be only a first step in the nozzle shortening. It is presently considered to start the De Laval extension inside the F4 nozzle. Two different solutions may be used:

- Machine the tungsten part of the lengthened F4 nozzle according to the bell-contoured profile.
- Machine the tungsten part of the nozzle cylindrically and insert the copper extension inside the F4 nozzle.

2.2 Additional Cooling Circuit

The copper De Laval extension must be cooled to prevent any overheating. The use of a secondary water circuit was thus decided. Figure 3 presents a computer-aided design (CAD) view of the turnaround duct that was welded (brazed) on the nozzle extension. Additionally, nonemerging holes were drilled at three different axial positions along the copper extension and thermocouples were placed in these holes to control the nozzle extension temperature. These three holes were filled using a refractory material after the thermocouple positioning. In practice, the temperature range measured by these thermocouples was always between 120 °C (pure argon plasma) and 270 °C (argon-hydrogen mixture).

Figure 4 shows a photograph of the experimental device in the vacuum chamber taken before the nozzle shortening. Currently, two different vacuum chambers were merged together for the significant lengthening of the plasma jet under very low pressure conditions.

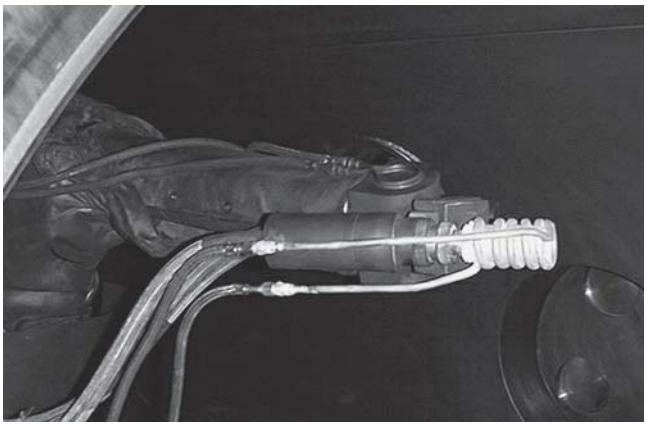

Fig. 4 Plasma gun fixed on the robot arm in the vacuum chamber (before the nozzle shortening)

3. Plasma Temperature Measurements

As it was said previously, difficulties were encountered concerning the powder injection (atomized CuAgZr powder +10-63 μm elaborated at LERMPS, Belfort, France). In particular, a partial clogging of the nozzle was observed when the injection point was placed close to the nozzle throat. On the contrary, the thermal energy available in the plasma jet seems too low to melt the particles when the injection point was placed close to the exit of the nozzle extension. From these results, temperature measurements were performed at the nozzle exit to check the plasma temperature range. These measurements were performed by placing samples of different materials in bar or wire forms at the nozzle exit. One may thus obtain the order of magnitude of the plasma temperature by using different type materials. This method represents a first stage of analysis and provides a qualitative comparison of the different parameters investigated. However, the melting of samples placed at the nozzle exit under such low-pressure and high-speed flow conditions is a complex phenomenon so that the present measurements cannot be used for any quantitative analysis.

Materials such as aluminum, copper, thoriated tungsten, alumina, and zirconia were used for these measurements. Moreover, the measurements were performed for the standard F4VB nozzle and the bell-contoured extended nozzle before the nozzle shortening (see above). Additionally, two different plasma gas mixtures and two different electric arc current intensities were considered. The different samples were positioned vertically about 5 mm downstream of the nozzle exit just at the jet axis (position 1) and at about 5 mm from the nozzle edge (position 2)

corresponding to a radial distance of about 8 mm from the jet axis in the case of the 27 mm exit diameter bell-contoured nozzle. The second positioning was mainly used to observe the effect of a small radial displacement on the material melting. Concerning the design of the samples, quarters of cylinders were used for metallic bars (radius = 8 mm) and the cross section of all other samples was almost the same.

Table 1 summarizes the results obtained for the cases of a pure argon plasma (40 sLpm) and an argon/hydrogen plasma gas mixture (40/10 sLpm) for a chamber pressure of 5 mbars. A double asterisk means that the sample remains molten even if it is displaced from the plasma jet axis, whereas a single asterisk means that the sample must be placed at the plasma jet axis to obtain a good melting. A minus sign means that the sample could not be molten, and the absence of any sign means that the corresponding test was not performed. From these results, one may deduce that:

- The plasma jet temperature at the nozzle exit remains sufficiently high to melt copper (melting point of about 1100 °C) whatever the nozzle design and the plasma nature.
- The plasma temperature at the nozzle exit is not enough to melt the thoriated tungsten (melting point of 3400 °C), except if the standard conical nozzle is used with an argon/hydrogen plasma gas mixture.
- Concerning the bell-contoured extension, the plasma temperature is high enough to melt copper even for a pure argon plasma and may allow melting zirconia (melting point of 2600 °C) if the sample is placed just at the plasma jet axis for the Ar/H_2 mixture.

The next results concern the bell-contoured nozzle extension only. One has to be reminded that the diameter of the lengthened nozzle was 5 mm only (Ref 1), which is smaller than the value of 6 mm of the standard conical nozzle.

Table 2 summarizes the electrical parameters and thermal efficiencies that were measured experimentally. The indicated cooling power P_c is that measured for the torch water circuit only so that it does not include the losses in the secondary circuit presented in Fig. 3. Despite that, the measured thermal efficiency is very low (about 30%) in comparison with that measured for more conventional plasma torches (often around 55%). This may be explained by the 30 mm long constant diameter lengthening shown in Fig. 1. Thus this nozzle presents additional thermal losses due to its small throat diameter (5 mm) and to the presence of the constant area lengthening. This is the reason why a shortening of the constant diameter part was decided as it was shown in Fig. 2. Moreover, the cooling power of the secondary water circuit must also be taken into account.

3.1 Comparison with Some Analytical Results

The above results might be helpful for showing what happens in the diverging nozzle. From the gas flow rates and thermal power, the pressure remains quite high at the nozzle throat (higher than 600 mbar according to our model). Thus, the diverging nozzle allows accommodating the upstream pressure to that of the chamber. From the supersonic flow in the divergent nozzle, the temperature decreases along the nozzle and the velocity increases. Considering the low thermal efficiency of the torch (Table 2), the plasma temperature range is not really high at the exit of the constant diameter part of the nozzle (lower than 8000 K according to the authors' model). Moreover, the above experimental results (Table 1) indicate that the plasma temperature drops significantly in the diverging nozzle ($T_{exit} < 3400$ K in most cases). Under such low pressure conditions, the Knudsen number determines the degree of rarefaction of the plasma gas and subsequently the flow regime. The Knudsen number is defined as (Ref 4):

$$Kn = \frac{\lambda}{D} = \frac{1}{\sqrt{2}\,\pi\sigma^2 nD} = \frac{kT/\left(\sqrt{2}\,\pi\sigma^2 P\right)}{D} \qquad \text{(Eq 1)}$$

in which λ is the molecular mean free path, D is the characteristic length scale of the flow, σ is the molecular diameter, n is the molecule number density (m^{-3}) and T, P, and k are the pressure, temperature, and Boltzmann's constant (1.38×10^{-23} J/K), respectively.

The continuum assumption is appropriate for $0 < Kn < 0.001$, whereas the rarefaction effect starts to influence the flow in the slip-flow regime ($0.001 < Kn < 0.1$) (Ref 4). Nevertheless, in the slip-flow regime, the Navier-Stokes equations can still be used providing a slip-velocity boundary condition along the walls of the flow domain (Ref 4).

For the present conditions, the Knudsen number is the highest at the nozzle exit (less favorable case). Considering an approximate temperature of 2000 K, a molecular diameter of 3.4 Å (pure argon, Ref 5), a pressure of 10 mbar (value imposed hereafter in the computational fluid dynamic (CFD) modeling results computed with FLUENT), and the nozzle exit diameter of 27 mm, one may deduce a value of 0.002 for the Knudsen number. For this value, the continuum assumption may still be used as first approximation.

Table 1 Summary of the temperature measurements performed 5 mm downstream of the nozzle exit

	Standard conical nozzle				Bell-contoured nozzle	
	Ar		Ar/H_2		Ar	Ar/H_2
	500 A	700 A	500 A	700 A	700 A	700 A
Al	**	**	**	**	**	**
Cu	**	**	**	**	**	**
$WThO_2$	–	–	*	*	–	–
Fe						*
Al_2O_3						*
ZrO_2						*

*, sample must be placed at the plasma jet axis to obtain good melting; **, sample remains molten even if displaced from the plasma jet axis; –, sample could not be molten

Table 2 Electrical parameters and thermal efficiency of the torch for different conditions (measurements performed before the nozzle shortening)

	I, A	*U*, V	P_c, kW	eff, %
Ar (40)	600	32	13.2	31
	700	32	16.3	27
Ar/H_2 (40/10)	700	52	24.7	32

It is thus interesting to check if one of the two following assumptions (equilibrium or frozen flow) might explain the measured plasma temperature range at the nozzle exit. In principle, chemical recombinations occurring in the plasma help to maintain a high temperature under equilibrium conditions. On the contrary, one may expect a lower temperature for a frozen flow. Most of the time, isentropic relationships are provided in the literature for the case of a frozen flow. These equations apply well in many cases, such as the studies of the cold spray process. However, as it was pointed out by Zeleznik and Gordon in 1968 (Ref 6), these equations are often mistakenly used for reacting mixtures for which they do not apply. The derivation of the corresponding equations for a reactive flow is much less common. However, these equations were provided in Ref 1 and 7. For a given nozzle, the exit Mach number is linked to the exit/throat area ratio by the relationship:

$$\frac{A_e}{A^*} = \frac{1}{M_e}\left[\frac{2\alpha + (\gamma - 1)M_e^2}{2\alpha + (\gamma - 1)}\right]^{(\gamma+1)/[2(\gamma-1)]} \quad \text{(Eq 2)}$$

in which A_e and A^* are the exit and throat area and M_e is the exit Mach number.

In this equation, the two thermodynamic derivatives α and γ are defined as (Ref 1, 7):

$$\alpha = -(\partial \ln \rho / \partial \ln T)_P \quad \text{(Eq 3)}$$

and

$$\gamma = (\partial \ln P / \partial \ln \rho)_S \quad \text{(Eq 4)}$$

in which ρ, T, P, and S, respectively stand for density, temperature, pressure, and entropy. Once M_e has been calculated, the next relationships can be used to evaluate the other main characteristics of the flow:

$$\frac{P^*}{P_e} = \left[\frac{2\alpha + (\gamma - 1)M_e^2}{2\alpha + (\gamma - 1)}\right]^{\gamma/(\gamma-1)} \quad \text{(Eq 5)}$$

and

$$\frac{T^*}{T_e} = \left(\frac{P^*}{P_e}\right)^{1/\beta} \quad \text{(Eq 6)}$$

in which P^*, P_e, T^*, and T_e are the throat and exit pressure and temperature respectively, and

$$\beta = (\partial \ln P / \partial \ln T)_S = \frac{C_p}{nR\alpha} \quad \text{(Eq 7)}$$

where C_p is the specific heat at constant pressure in J/kg · K. (n is the number of moles per unit of mass, so that nR has also the unit of J/kg · K.)

By considering the case of pure argon presented in Table 2, a net thermal power of 6 kW may be deduced. Moreover, an estimation of the throat temperature may be obtained from the total enthalpy change from the gun inlet to the nozzle throat:

Table 3 Effect of the nozzle shortening on the torch thermal efficiency and thermal losses

		Lengthened		Shortened		
Ar-H_2 sLpm	I, A	U, V	Eff, %	U, V	Eff, %	P_e, %
40-2	600	43	32	42	46	−22
40-5	600	48	36	46	48	−22
40-7	700	52	32	52	42	−15

Eff, efficiency

$$h^* + c^{*2}/2 - h_o = P_e / Q_m \quad \text{(Eq 8)}$$

in which h^* and c^* are the specific enthalpy and sound velocity at the throat, h_o is the specific enthalpy at room temperature, P_e is the effective thermal power, and Q_m is the plasma gas mass flow rate. The throat temperature may then be estimated from the results of the authors' in-house software allowing the calculation of thermodynamic properties and transport coefficients of thermal plasmas up to 20,000 K and providing tabulated data of $h + c^2/2$ as a function of the temperature (Ref 8). A value of $T^* \approx$ 7520 K may thus be estimated with this method. This value is quite small because of the low thermal efficiency measured for this case. From the low plasma ionization rate obtained, the corresponding thermal derivatives are not significantly different from those obtained for a nonreactive flow (γ = 1.59 instead of 1.67, α =1.01 instead of 1, and β =2.72 instead of 2.5).

Applying Eq 2, 5, and 6 (isentropic relationships) to that case, one may deduce a temperature lower than 1000 K at the exit of the bell-contoured nozzle using the equilibrium assumption (and even lower for the frozen one). In fact, from the large thermal losses of the torch cooling water circuit, the thermal power available in the plasma is very low and the plasma ionization rate is not sufficient to produce thermodynamic derivatives sufficiently different from that obtained for a frozen situation. In other words, chemical recombinations occurring in the plasma are not sufficient to maintain its temperature to a high level. Thus, one may suppose that only nonequilibrium phenomena may explain the copper fusion at the De Laval nozzle exit for these conditions. However, the presence of a stagnation point at the surface of the sample placed in front of the jet may distort this conclusion since the total temperature may exceed the material melting point, although the static one does not. Moreover, the influence of the low pressure on the material melting temperature was not taken into account, but it is negligible.

3.2 Effect of the Nozzle Shortening

Some new experiments were performed before and after the nozzle shortening (Fig. 1, 2). Since a new cathode was used for these measurements, the results were slightly different from that presented in Table 2. The bell-contoured nozzle extension was not attached to the anode during these experiments. Table 3 presents the effect of the nozzle shortening on the torch thermal efficiency for different parameters. The measured thermal efficiency ranges between 32 and 36% for the lengthened nozzle and between 42 and 48% after the nozzle shortening. The thermal losses decrease by more than 20% due to the nozzle shortening. A noticeable amount of energy is thus saved.

From the aforementioned results, the shortening of the lengthened nozzle (Fig. 2) should therefore allow improving the

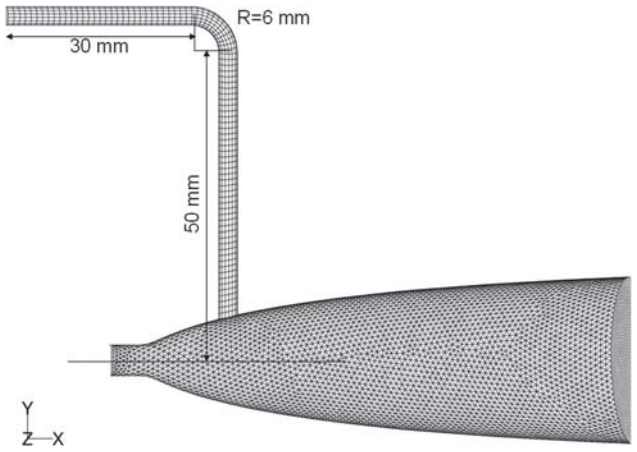

Fig. 5 View of the unstructured type grid

melting of the particles injected in the plasma jet. However, since clogging was observed using the lengthened nozzle equipped with the De Laval extension, particular attention must be paid to the injection point location.

4. Modeling of Particle Injection

The present part of the work was performed to consider the position of the injection point in the De Laval extension. Three different cases were studied. The CFD model was implemented within FLUENT software package (Lebanon, NH). The calculation domain includes the bell-contoured diverging nozzle and the powder injector. The injector presents an internal diameter of 3 mm, a vertical part of 50 mm, a bend with a curvature radius of 6 mm, and a horizontal part of 30 mm, as shown in Fig. 5. The plasma mass flow rate and total temperature were imposed at the nozzle throat (main inlet of the computational domain) and at the inlet of the carrier gas, whereas a fixed pressure boundary condition was applied at the nozzle exit (10 mbar). A zero flux boundary condition was applied for the carrier gas injector wall, and a temperature of 400 K was considered for the bell-contoured nozzle wall. The plasma specific heat was calculated assuming a frozen flow in the diverging nozzle, and the transport properties (viscosity and thermal conductivity) were read in a data file containing the properties of the pure argon plasma versus temperature (Ref 8). The grid was formed by prisms (extruded triangles) in the powder injector and tetrahedrons in the bell-contoured De Laval nozzle. From the presence of a symmetry plane, only one-half of the geometry was represented and the total number of cells was 89,000.

Figure 6 presents the computed absolute pressure, density, velocity, Mach number, and total temperature contours in the symmetry plane of the De Laval extension for an injection point placed at 14 mm beyond the throat and a carrier gas flow rate of 2 sLpm. The considered thermal efficiency of the torch (45%) was measured for the shortened nozzle of Fig. 2 so that an effective power of 10 kW was used (instead of 6 kW for the lengthened nozzle as mentioned previously). A logarithmic color scale was used for pressure and density to improve the picture readability. The pressure ranges between 875 Pa in the diverging nozzle and 73,500 Pa at the nozzle throat. The density is the highest in powder injector (0.126 kg/m^3) and the lowest at the nozzle exit. The maximum computed velocity is 3360 m/s, and the maximum value of the Mach number is a little more than 4. Concerning the total temperature, it comprises between 285 K in the powder injector and 14,000 K at the nozzle throat. The maximum value of 14,000 K corresponds to an absolute temperature of 10,600 K.

A multiparticle injection model was used to investigate the particle flux deviation provided by the plasma flow. This model was used to check the differences concerning the particle flux deviation for different injection positioning. The authors' objective was not to quantify the particle velocity and temperature at the nozzle exit so that no special effort was paid to the development of this model in these circumstances. A one-way model calculating the effect of the flow on the particles and a two-way coupling (taking also the effect of the particles on the flow into account) were alternatively used. The use of the second model indicates that the particles may act significantly on the plasma flow fields (velocity, temperature, and so forth) depending on the powder mass flow rate. Figure 7 presents the computed particle trajectories in the diverging nozzle and the powder injector calculated with the one-way model. The color scale was set for the particle size (in m) for which a Rosin-Rammler distribution was assumed. According to this model, the volume fraction y_d of particles of diameter greater than d is given by:

$$y_d = e^{-(d/\bar{d})^n} \quad \text{(Eq 9)}$$

Finally, a mean value of 30 μm was considered with a dispersion parameter n of 2 and a size distribution ranging between 10 and 60 μm.

The computed pressure within the carrier gas injector was 98 mbar (relative pressure), and the corresponding carrier gas velocity was about 47 m/s. Thus, a particle injection velocity of 30 m/s was assumed at the inlet of the carrier gas injector (top-left side of Fig. 5). The numerical results suggest that many collisions occur within the powder injector, in which the particle trajectories seem particularly random. However, collisions with the injector walls were supposed elastic so they do not contribute to slowing down the particles. As it was expected, a size-dependent particle segregation is observed. The smallest particles are found close to the nozzle axis, whereas the largest ones impinge the nozzle edge at the opposite side of the injector (28% of the total number of particles). Concerning the other predicted particle characteristics, their velocities range between 150 and 900 m/s and their temperature between 600 and 2200 K at the nozzle exit due to the spread particle size distribution that was taken into account.

Figure 8 presents the predicted trajectories obtained for the second injection point (i.e., translation of 20 mm in the X direction). In this calculation, the inlet particle velocity was not changed (i.e., 30 m/s), although the computed pressure in the injector was lower (58 mbar instead of 98) and the corresponding carrier gas velocity was higher (75 m/s instead of 47). Thus, although the particle injection velocity was not increased, the

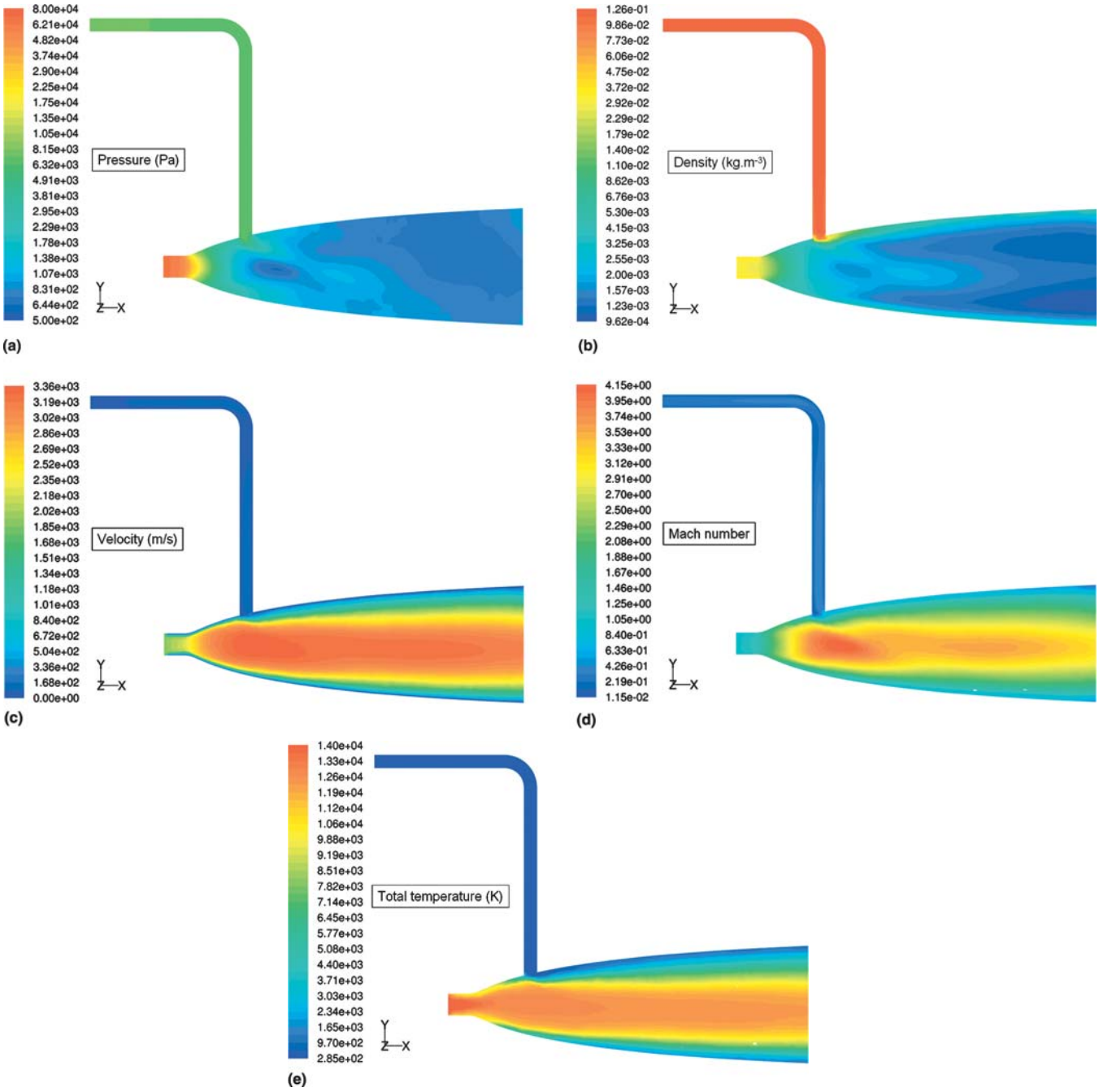

Fig. 6 Computed pressure, density, velocity, Mach number, and total temperature fields in the bell-contoured extension (Ar, 40 sLpm, 700 A, eff = 46%). (a) Pressure in Pa. (b) Density in kg/m^3. (c) Velocity in m/s. (d) Mach number. (e)Total temperature in K

particles seem much less deviated by the plasma flow so the largest particles still impinge the nozzle edge at the opposite side of the powder injector for this new position of the injection point (32% of the total number of particles). One may expect that the particles would be even less deviated if a larger injection velocity had been considered. Moreover, the particle velocity at the nozzle exit is lower for this second case (150 to 700 m/s) and the temperature is lower as well (500 to 1500 K).

The major problem of the present model is that the temperature of the particles that impinge the nozzle edge (i.e., the largest particles) do not exceed the powder melting point according to the present modeling results, whereas clogging is observed during experiments. This discrepancy certainly comes from the frozen assumption that overestimates the temperature drop in the bell-contoured nozzle extension. An improvement of the model is thus required to predict more accurately the particle heating in the diverging nozzle. Concerning the last position of the injection point, clogging is never obtained (for both experiments and modeling results). However, in this case, the particle melting is never reached.

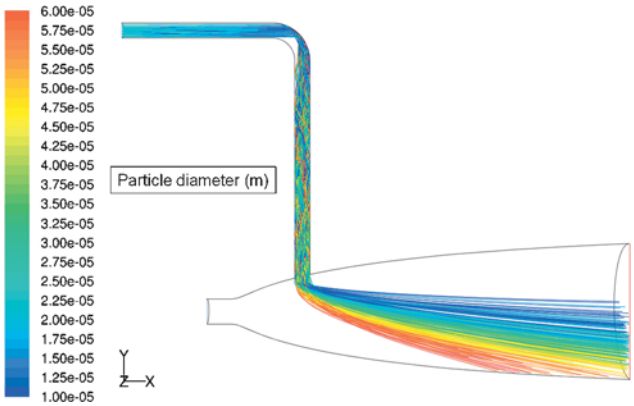

Fig. 7 Computed particle trajectories in the bell-contoured nozzle extension (color scale for particle diameter in m)

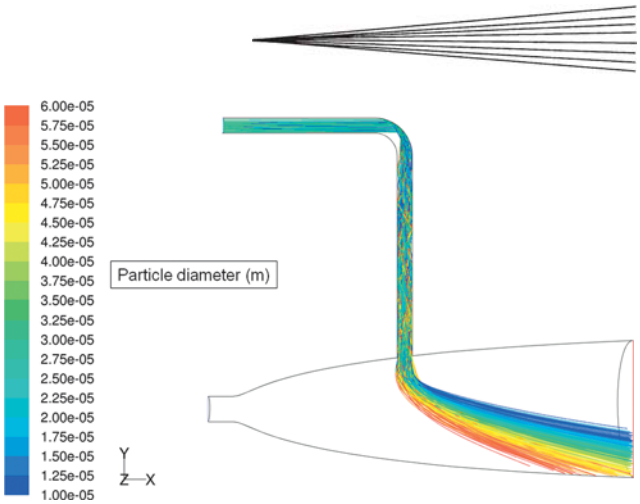

Fig. 8 Computed particle trajectories in the bell-contoured nozzle extension (case of the second injection point placed at 34 mm from the throat, color scale for the particle diameter in m)

5. Conclusions

This study was devoted to presenting the authors' latest developments concerning the use of a bell-contoured nozzle extension for thermal spray under very low pressure conditions. A lengthened F4 type nozzle was shortened by 28 mm (Fig. 2) to decrease thermal losses to the torch cooling water circuit (−20%). An in-house bell-contoured extension was attached to the torch, and a secondary water circuit was brazed around it (Fig. 3). Some samples of different materials in bar or wire forms were placed at the nozzle exit to estimate the plasma temperature range. Finally, some modeling results were performed to study the influence of the powder injector positioning. The computed particle trajectories can explain the nozzle clogging in each case. However, the model tends to underestimate the particle temperature due to the frozen assumption that was used for the flow study. A change in the powder injector design could be considered during 2006 to try to decrease the particle injection velocity and avoid the nozzle clogging. Moreover, the use of an axial injection would certainly be more efficient for the present process.

References

1. R. Bolot, D. Klein, and C. Coddet, Design of a Nozzle Extension for Thermal Spray under Very Low Pressure Conditions, *Thermal Spray Solutions: Advances in Technology and Application,* May 10-12, 2004 (Osaka, Japan), DVS, 2004
2. K. Foelsch, The Analytical Design of an Axially Symmetric Laval Nozzle for a Parallel and Uniform Jet, *J. Aeronaut. Sci.,* 1949, p 161-166
3. D.E. Sokolov, S.O. Chwa, D. Klein, C. Coddet, and P. Nardin, Coatings Obtained by Low Pressure Plasma Spraying, *Thermal Spray Connects: Explore Its Surfacing Potential,* May 2-4, 2005 (Basel, Switzerland), DVS, 2005
4. R.W. Barber and D.R. Emerson, The Influence of Knudsen Number on the Hydrodynamic Development Length within Parallel Plate Micro-Channels, *Advances in Fluid Mechanics IV,* M. Rahman, R. Verhoeven, and C.A. Brebbia, Ed., WIT Press, Southampton, U.K., 2002, p. 207-216
5. J.O. Hirschfelder, C.F. Curtiss, and R.B. Bird, *Molecular Theory of Gases and Liquids,* 4th ed., John Wiley & Sons, New York, London, Sydney, 1967
6. F.J. Zeleznik and S. Gordon, Calculation of Complex Chemical Equilibria, *Ind. Eng. Chem.,* 1968, **60**(6), p 27-57
7. R. Bolot, D. Klein, and C. Coddet, Influence of the Nozzle Design on the Structure of a Plasma Jet under Vacuum Conditions, *Tagungsband Conference Proceedings,* March 4-6, 2002 (Essen, Germany), E. Lugscheider, Ed., DVS, 2002, p 938-943
8. R. Bolot, "Modélisation des écoulements de plasmas d'arc soufflé: Application à la projection de matériaux pulvérulents," thesis, University of Franche-Comté, France, No. 42, 1999, in French